CORE
Metadata, citation and similar papers at core.ac.uk
Provided by Digital Commons @ West Chester University

West Chester University
Digital Commons @ West Chester University

Chemistry | College of Arts & Sciences

2-6-2015

The stoichiometry of metal assisted etching (MAE) of Si in V2O5 + HF and HOOH + HF solutions

Kurt W. Kolasinski
West Chester University of Pennsylvania, kkolasinski@wcupa.edu

William B. Barclay
West Chester University of Pennsylvania

Yu Sun
University of Connecticut - Storrs

Mark Aindow
University of Connecticut - Storrs

Follow this and additional works at: http://digitalcommons.wcupa.edu/chem_facpub

Part of the Materials Chemistry Commons

Recommended Citation

Kolasinski, K. W., Barclay, W. B., Sun, Y., & Aindow, M. (2015). The stoichiometry of metal assisted etching (MAE) of Si in V2O5 + HF and HOOH + HF solutions. *Electrochimica Acta*, 219-228. http://dx.doi.org/10.1016/j.electacta.2015.01.162

This Article is brought to you for free and open access by the College of Arts & Sciences at Digital Commons @ West Chester University. It has been accepted for inclusion in Chemistry by an authorized administrator of Digital Commons @ West Chester University. For more information, please contact wcressler@wcupa.edu.

*Revised Manuscript (including Abstract)
Click here to view linked References

The stoichiometry of metal assisted etching (MAE) of Si in V_2O_5 + HF and HOOH + HF solutions

Kurt W. Kolasinski,[a]* *William B. Barclay,*[a,†] *Yu Sun*[b] *and Mark Aindow*[b]

[a] Department of Chemistry, West Chester University, West Chester, PA, 19383-2115 USA

[b] Department of Materials Science and Engineering, and Institute of Materials Science, University of Connecticut, Storrs, CT 06269-3136

*Corresponding author

KEYWORDS silicon nanowires, metal assisted etching, metal nanoparticles, surface chemistry.

The metals Ag, Au, Pd and Pt were deposited as nanoparticles onto H-terminated Si(100) wafers and single crystal Si chunks to act as catalysts for electroless etching induced by the presence of a strong oxidant in HF(aq). This process is known as metal assisted etching (MAE). Aqueous solutions of V_2O_5 + HF and HOOH + HF were investigated. The stoichiometry of MAE in V_2O_5 + HF solutions depended on the chemical identity of the metal. The stoichiometry when etching with Ag and Au was the same as previously determined for electroless Si etching in V_2O_5 + HF solutions in the absence of a metal catalyst. With Pd and Pt nanoparticles the stoichiometry is significantly different, consuming more V_2O_5 and producing less H_2 per mole of Si etched. This indicates that the metal catalyst changes the mechanism of etching, implicating the polarization induced by the metal nanoparticle in the etch mechanism. Etching in V_2O_5 + HF was well behaved and gave consistently reproducible kinetic results. In contrast, we were unable to obtain well-behaved stoichiometries for HOOH + HF solutions. This is related to heightened sensitivity on reaction conditions compared to the V_2O_5 system as well as nonlinearities introduced by side reactions.

Keywords: Silicon nanowires, porous silicon, metal assisted etching, surface chemistry; reaction mechanism

AUTHOR INFORMATION

Corresponding Author

*kkolasinski@wcupa.edu

Present Addresses

†Department of Chemical and Biological Engineering, University of Maine, Orono, ME 04469, USA

Introduction

Electroless etching of silicon in fluoride solutions is an extremely versatile process that is capable of producing planar, porous and nanowire structures [1]. When performed in a regime that produces microporous silicon it is commonly called stain etching [2,3], a process known since the work of Fuller and Ditzenberger [4], Turner [5] and Archer [6]. A metal catalyst can be used to modify the etching process. This was first recognized in a controlled manner by Kelly and co-workers, who coined the term galvanic etching to describe the catalytic etching of silicon induced by planar metal structures [7,8]. Bohn and co-workers [9,10] advanced the range of accessible morphologies by introducing the metal as random or patterned nanoparticles. This process is known as metal assisted etching (MAE).

Metal assisted etching has attracted increasing attention because it is extremely adept at producing either porous Si (por-Si) [11] or Si nanowires (SiNW), potentially in ordered arrays [12-14] depending on the initial geometry of the deposited metal [15-19]. Silicon nanowires exhibit interesting electrical and optical properties [20-22] and are of considerable interest for applications in thermoelectrics [23], sensing [24,25], photovoltaics and photoelectrochemistry [26-29], surface functionalization [30] (including formation of superhydrophobic surfaces) [31], catalysis [32], nanoelectronics [33-37], and energetic materials [38]. An improved mechanistic understanding of the chemistry involved in metal assisted etching is vital to achieving more reproducible and controlled nanostructure formation.

Understanding of the chemistry fundamental to stain etching has advanced greatly as a result of quantitative studies on charge transfer and reaction stoichiometry [39-42]. Anodic etching in the por-Si formation region occurs either by a current doubling (valence 2) or current quadrupling (valence 4) path. An electropolishing regime (valence 4) is also observed at high bias [43,44]. Kolasinski and Barclay demonstrated [39] that etching of Si in a solution composed of V_2O_5 dissolved in HF(aq) proceeds with a stoichiometry given by a half-reaction with *valence 2*

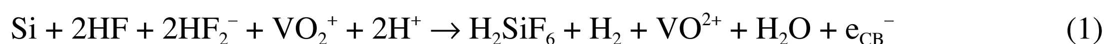

$$Si + 2HF + 2HF_2^- + VO_2^+ + 2H^+ \rightarrow H_2SiF_6 + H_2 + VO^{2+} + H_2O + e_{CB}^- \qquad (1)$$

accompanied by a charge balancing counter reaction

$$VO_2^+ + 2H^+ + e_{CB}^- \rightarrow VO^{2+} + H_2O. \qquad (2)$$

In other words, two moles of the oxidant VO_2^+ are consumed and one mole of H_2 is produced per mole of Si etched. This is different than the stoichiometry observed in anodic etching of Si in the por-Si formation regime. However, it is completely consistent with a quantitative evaluation of charge transfer rates based on Marcus theory. This stoichiometry makes sense because the rate of conduction band electron transfer into VO_2^+ via reaction (2) greatly exceeds that of the rate of conduction band electron transfer into H^+ via reaction (3).

$$H^+ + e_{CB}^- \rightarrow 1/2\ H_2 \qquad (3)$$

According to Marcus theory, the rate of electron transfer from the conduction band is proportional to the hopping probability factor W, which depends on the electrochemical potential of the oxidant E_{ox} according to

$$W(E_{ox}) = \exp\left[-\left(\left(E_C - E_{ox} + \lambda\right)^2 / 4\lambda k_B T\right)\right]. \qquad (4)$$

Silicon etching in HF solutions is extremely exothermic [42] and its rate is controlled by the rate of hole injection into the Si valence band [40,42,44,45]. Any oxidant that can efficiently extract electrons from the Si valence band – a prerequisite for effective stain etching – must have an electrochemical potential more positive than roughly +0.7 V so that its acceptor level overlaps with the Si valence band. VO_2^+ with $E° = 0.91$ V lies approximately 1 eV below the Si conduction band edge. Thus, not only is VO_2^+ well suited to accept valence band electrons, but also conduction band electron transfer into VO_2^+ is near the optimal value. H^+ at $E° = 0$ V lies just a few tenths of an eV below the conduction band minimum E_C [40,42] and well above the valence band maximum.. While it is thermodynamically possible for H^+ to act as an oxidant for Si etching, it is kinetically inhibited from doing so. Furthermore, its acceptor level is poorly positioned compared to VO_2^+, and it must have a lower rate of charge transfer from the conduction band. This comparison will hold for any stain-etchant-inducing oxidant that is stable in an aqueous solution [39].

For etching in the presence of a metal, we need to consider the effect of the metal on charge transfer as well as on its potential role as a catalyst. A solution of HOOH + HF does not etch Si at an appreciable rate, much less than 0.01 nm s^{-1} at the concentrations used in this study [46,47]. However, HOOH + HF is the most commonly used solution for MAE. Therefore, a fundamental question to ask is, since we know that the metal (by density of states arguments) can change the kinetics of the charge transfer, does the metal act only as a catalyst or does it also affect the etch mechanism? Furthermore, is the etch mechanism influenced by the chemical identity of the metal?

We have chosen a range of metals that differ with respect to their catalytic character. A good hydrogen recombination catalyst (1) has a d band that straddles the Fermi energy, (2) does not bind H atoms too strongly, and (3) does not present a barrier to H_2 dissociation [48,49]. Si fails on all three counts and is an inferior catalyst. Ag and Au are also poor hydrogen recombination catalysts, though they are still more effective than Si. Both bind H atoms weakly and present a barrier to H_2 dissociation. Pd and Pt are excellent hydrogen recombination catalysts.

In this report we explore the deposition of Ag, Au, Pd and Pt onto H-terminated Si and then compare etching induced by either V_2O_5 or HOOH dissolved in HF(aq) to etching in the absence of the metal. In general, metals deposited by galvanic displacement on Si do not adhere strongly to the surface. Therefore they tend to form clusters or dendrites of various shapes depending on the deposition conditions, such as temperature, pH, concentration and deposition time [50]. We find that the stoichiometry of etching in V_2O_5 + HF depends on the metal used as a catalyst. Just as for etching in the absence of metal, etching in the presence of Ag and Au nanoparticles exhibits molar ratios of roughly 2:1 for $n(\mathrm{VO_2^+})/n(\mathrm{Si})$ and approximately 1:1 for $n(\mathrm{H_2})/n(\mathrm{Si})$. Therefore, even though the photoluminescence (PL) and structure of these films is different from films produced in the absence of the catalyst, the mechanism of etching is the same. Put differently, the spatial character of etching is different with and without the presence of Ag or Au, but the chemistry itself does not change.

Etching in the presence of Pd and Pt nanoparticles exhibits decidedly different stoichiometries. For Pt, $n(VO_2^+)/n(Si) \approx 4$ and $n(H_2)/n(Si) \approx 0$. Pd etches initially with the same stoichiometry as Pt; however, as time passes it tends toward $n(VO_2^+)/n(Si) \approx 3$ and $n(H_2)/n(Si) \approx 0.5$. Therefore, the introduction of a good hydrogen recombination catalyst changes the mechanism of etching as compared to stain etching.

We were unable to obtain similarly well-behaved kinetic data from HOOH-initiated etching. This system is inherently more chaotic. We believe this is caused by much greater sensitivity to reaction conditions and the interference of competing reactions involving H_2, O_2, H_2O and HOOH.

Experimental

Etching was performed on Si(100) 0–100 Ω cm *p*-type test grade wafers (University Wafers) or unpolished single crystal reclaimed wafer chunks (Union Carbide). Wafers and chunks were used for SEM and PL studies, whereas chunks were used exclusively in kinetics studies. Polished wafers could not be used for kinetics studies because of their low surface area. The wafer chunks represent a moderate surface area (high compared to wafers, low compared to powder) and high purity sample. Chunks were sieved to obtain a narrow size distribution (3.35–4.75 mm) and a large enough sample size was used (1–2 g) to ensure constant initial surface area. Roughly 2–3% of this mass is etched during experiments. Silicon was cleaned by ultrasonication in acetone (Pharmco-Aaper HPLC/UV grade) then ethanol (Pharmco-Aaper anhydrous ACS/USP grade) followed by rinsing in water. After etching, samples were rinsed in water (deionized and distilled) and ethanol, then dried either in a stream of Ar gas or in CO_2 + ethanol mixtures using a Tousimis AutoSamDri 815 critical point drier. V_2O_5 (Fisher certified grade), HOOH (Columbus Chemical Industries 3% solution in water) and HF (JT Baker 49% analytical grade) were used to create stain etchants. Concentrated HF was diluted 1:3 with water. The concentration of

V_2O_5 was 0.012 M for UV/Vis experiments and 0.045 M in H_2 evolution experiments. HOOH etchant was composed of 2:5:30 solution of 3% HOOH : 49% HF : H_2O.

Secondary electron scanning electron microscopy (SEM) images were obtained in an FEI Quanta 400 Environmental SEM operating at 20 kV in high vacuum mode and using an Everhardt-Thornley detector. Higher resolution SEM images were acquired using the electron column in an FEI Strata 400S dual-beam focused ion beam apparatus. This latter instrument was operated at an accelerating voltage of 10 kV and the secondary electron signals were collected using a through-the-lens detector. Cross-sectional samples for transmission electron microscopy were prepared in the dual-beam instrument using the Ga ions column. The samples were examined in an FEI Tecnai T12 TEM operating at 120 kV. Absorption spectroscopy for kinetics experiments was performed on a Cary 300 Bio UV/Vis spectrometer. Digital pressure, temperature and time data were recorded with a MicroLAB 4205 unit interfaced to a computer. Hydrogen evolution was monitored by measuring the pressure in a reaction vessel composed of two 750 mL high-density polyethylene (HDPE) Erlenmeyer filter flasks connected by a short section of Tygon tubing. Both the reaction and ballast flasks were stoppered and submerged in a thermostated bath. The ballast flask was connected through its stopper by a thin Teflon tube to the pressure sensor. Photoluminescence spectra excited at 350 nm were acquired on a Cary Eclipse fluorescence spectrometer with the slits set on both excitation and emission monochromators for 5 nm resolution. The excitation light is incident at 45°. A handheld Way Too Cool 9 W UVC lamp with primary emission near 250 nm was used for visual inspection of photoluminescence.

Our initial efforts at depositing metal layers were performed with a Cressington sputter coater. The results were very poor, subject to lift off of the metal layer, and yielding irreproducible kinetics and film structure. Infrared spectroscopy revealed that metal layers produced in this manner are easily contaminated with hydrocarbons due to exposure to the atmosphere.

Therefore we switched to a technique that involved formation of a H-terminated Si surface followed immediately by metal deposition and etching without exposure of the H-terminated or metal-deposited surface to the atmosphere. Metal deposition was performed with an Ar buffer layer blown into the beaker by stripping the oxide from a clean Si wafer in concentrated HF to make a H-terminated Si surface. An appropriate number of drops of ~3 mM metal salt solution was added to HF to deposit a quantity of metal corresponding to a uniform coverage of 10nm in thickness. As we show below, the metals form clusters rather than flat films. The cleaned Si wafers were transferred directly from the water rinse solution to HF for oxide stripping and metal deposition with a droplet of water covering the wafer. After 15 min in the deposition solution, the Si wafers with metal deposits were transferred directly to the stain etchant while still wet to avoid atmospheric contamination. As will be shown below, *it is critical for reproducible results that the deposited metal layers are not dried in air before etching*. If allowed to dry in air, deposited metal nanoparticles tend to agglomerate. For some SEM and PL studies an oxidant containing solution was added directly to the deposition solution. In either case, the H-terminated surface and the deposited metal nanoparticles were never exposed to the atmosphere nor subjected to drying. Aqueous salt solutions used for deposition include $PdCl_2$ (Sigma-Aldrich, reagent plus, 99%), $AgNO_3$ (ACS certified, >99.7%), $HAuCl_4$ (Sigma-Aldrich, 200 mg dl^{-1}) and H_2PtCl_6 (EMD Chemical, 10% (w/w) solution).

V_2O_5 dissolves in HF to produce VO_2^+. This is reduced during por-Si formation to form VO^{2+}. The decrease in concentration of the V(V) species VO_2^+(aq) and the increase in concentration of the V(IV) species VO^{2+}(aq) were simultaneously monitored by UV/Vis spectroscopy. A quantitative correspondence in the decrease in VO_2^+(aq) and increase in VO^{2+}(aq) concentrations described by a single rate constant indicates that no side reactions occur during stain or metal assisted etching. We used V_2O_5 + 1:3 HF:H_2O to form the etchant for kinetics studies. Therefore, we must use polymethylmethacrylate (PMMA) cuvettes for absorption spectroscopy and Beer-Lambert analysis. We

used $VOSO_4$ (Strem) dissolved in 1:3 HF:H_2O to provide a standard for the VO^{2+} absorption spectrum. Further details pertaining to experimental and data analysis procedures have been reported elsewhere [51].

Results

Metal Deposition

We investigated the state of the metal particles before etching with electron microscopy. Metal was deposited galvanically from solution as detailed above. In our first series of experiments, the samples were rinsed once in 1:1 water:ethanol and three times in ethanol solutions. They were then blown dry with a stream of Ar. Typical SEM images and particle size distributions for Ag and Pd deposited and dried in this manner are shown in Fig. 1 (a)–(d). Particularly in the case of Ag, there was evidence for the agglomeration of much smaller clusters into larger clusters. This was also the case for Pd, though the agglomeration was less severe. The majority of Ag clusters were <100 nm in diameter. Larger clusters were clearly composed of aggregations of smaller particles and the long tail in the distribution brought about by the larger clusters increased the mean cluster diameter to 110 nm. A more symmetrical distribution centered about 47 nm was observed for Pd. We can conclude with certainty that the nascent cluster size distributions for Ag and Pd were significantly smaller than those presented in Fig. 1. The agglomeration effect was consistent with very weak adhesion of Ag and Pd clusters to the Si surface, which has been reported in the literature [50,52,53].

Similar preparation conditions were simply inadequate for the observation of Au and Pt clusters. If the samples were dried with Ar after deposition of Au and Pt, SEM images revealed that clusters had been completely removed from large areas of the surface. The vast majority of the deposited metal was either removed entirely from the surface or displaced into large debris piles. In order to investigate the nascent size distribution of the deposited Au and Pt clusters, we changed our rinsing protocol. The images and distributions displayed in Fig. 1 (e)–(h) were obtained after rinsing four times in ethanol. The samples were placed in a Teflon cup for transfer from one solution to the next so that they never were dried

between rinsing steps. After the fourth rinse, the Teflon cup was then introduced into a critical point drying apparatus. Critical point drying in CO_2 was then performed. Well-dispersed and very small nanoclusters were then observed. Pt exhibited a symmetrical distribution much like Pd but narrower and centered at 33 nm. The Au distribution was displaced toward much smaller clusters with a mean diameter of only 10 nm.

Previous studies [50,52,53] of galvanic metal deposition on Si have reported that the deposited metals adhere poorly to the Si surface. This is consistent with the very weak adhesion we observed. These previous studies, as well as other reports [11,54-62] of nanoparticle formation, dried their samples in air, with streaming gas, or did not specify their drying conditions. Our results suggest that the use of critical point drying is essential for obtaining accurate nanoparticle size distributions and that previous conclusions regarding size distributions and their dependence on deposition parameters may need, in some cases, to be reevaluated.

While the distributions shown in Fig. 1 are not the nascent distributions in the case of Ag and Pd, they nonetheless demonstrate that the deposited metal exists prior to etching as isolated nanoparticles rather than a continuous film. Furthermore, the nanoparticles primarily (perhaps exclusively in the absence of aggregation) exhibit diameters below 100 nm and cover roughly 5% of the surface area of the substrate.

Observation of Etch Progress and Photoluminescence of Si Wafers

After metal deposition there were no obvious changes to the appearance of the Si crystals. This was consistent with the low coverage of nanoparticles expected from the deposition conditions. Before the addition of oxidant, it was clear that the behavior of a Pd coated sample was different than the samples coated with other metals. Silicon crystals upon which Ag, Au and Pt have been deposited maintained their mirror finish and did not evolve any bubbles. If the Pd coated Si was allowed to sit for an extended period, the surface roughened, losing its mirror finish and a small quantity of bubbles was found. This behavior was consistent with that reported by Matsuda and co-workers [63], who found high catalytic activity for Pd nanostructures on Si in HF even in the absence of an oxidant. They attributed this low

level of reactivity to the effects of dissolved O_2. They also reported that this does not lead to por-Si formation. We confirmed the lack of microporous Si formation by photoluminescence (PL) measurements, or rather, the absence of PL under ultraviolet excitation.

After the addition of dissolved V_2O_5, reaction clearly occurred. The nature of the reaction depended on whether metal was present and the chemical identity of the metal. The addition of dissolved V_2O_5 in the absence of metal (conventional stain etching) led to very low bubble production. Bubbles often formed at the edges of the crystal and slowly grew in size before detachment. Crystals developed colors that swept across the surface and changed as etching proceeds. Only for extended etch times of 30 min or more did the surface lose its mirror finish and a rough surface appeared. These observations have been described previously and the smoothness or roughening of the layers has been confirmed by SEM measurements [40-42,64].

In the presence of metal, bubble formation and color changes were dramatically different. Bubbles immediately streamed off of the Ag-coated surface. The bubbles were very small and emanated from the entire crystal face. The color changed rather uniformly; however, after an initial burst of vibrant colors, the Ag-coated samples soon became quite dark. The dark surface maintained mirror like properties for short etches but eventually became quite rough. Au-coated Si behaved similarly; however, the response was somewhat delayed compared to the Ag-coated samples. Pt-coated samples exhibited rapid color change initially then darkening and roughening. Bubble production was much reduced, with larger bubbles that tended to stick to the sample.

Brilliant visible PL was observed from films etched in the presence of Ag, Au and Pt nanoparticles. The PL was green-yellow-orange depending on several factors. Figure 2 displays the PL spectrum of a film etched in V_2O_5 + HF on a Pt-coated Si(100) wafer. Minimal exposure to the atmosphere ensured by placing the sample in an Ar purged desiccator until the PL spectrum was measured. This sample was deep green to the eye when excited by a handheld UV lamp. The PL peaks at 570 nm with excitation at

350 nm. The green PL was more persistent than what we have previously reported for conventional stain etching [65]. Green PL from stain-etched por-Si was stable as long as the samples were held in water. After a few minutes to an hour of air exposure, the green PL converted to the more usual orange PL. Green PL from metal assisted etching with V_2O_5 often persisted for several days or even weeks before evolving into the usual orange PL.

The behavior of Pd-coated samples was completely different. The surface of the sample did not exhibit color change – they simply darkened and roughened. Bubbles did not stream off. Instead they developed slowly and formed larger attached bubbles. No visible or infrared PL was observed unless etching was performed for extended periods of time (>60 min). Therefore, no microporous silicon was formed initially even though etching clearly occurred. Etching was clearly indicated both by the roughening of the sample and by the appearance of a blue color in the etch solution as VO_2^+ was converted to VO^{2+}.

The behavior was much different when HOOH was added as an oxidant instead of V_2O_5. In the absence of deposited metal, no reaction occurred with HOOH. This is consistent with previous results [15]. Even though allowed on energetic grounds (the HOOH donor level lies below the Si valence band maximum), the kinetics of charge transfer is very slow and requires a metal to catalyze the reaction of HOOH with Si. The need for a catalyst means that the HOOH must specifically adsorb on the surface of the metal before charge transfer can occur. If nonspecific adsorption were sufficient, there would be no barrier to direct hole injection into Si. We can infer this because we have previously shown [40] that Marcus theory quantitatively described the rate of hole injection of VO_2^+, Fe^{3+}, Ce^{4+} and $IrCl_6^{2-}$, all of which must therefore nonspecifically absorb on the Si surface before hole injection.

When HOOH was added to metal-coated Si samples immersed in HF(aq), etching was immediate in all cases. Small bubbles streamed off the surface from the entire surface. Samples immediately roughened. Ag- and Au-coated samples tended to take on more of a tan color as opposed to the darker brown or even black appearance of Pd- and Pt-coated samples. Samples exhibit visible PL, which has a

long tail into the IR, much longer than observed for metal assisted etching with V_2O_5. A typical spectrum from a sample etched into a Pt-coated wafer is shown in Fig. 2. The PL peaks around 615 nm and extends beyond 850 nm.

Structure of Etched Si Chunks

Silicon chunks are single-crystalline pieces of reclaimed Si wafers. As shown in Fig. 3(a), they are initially rough and exhibit multiple facets resulting from cleavage. Stain etching in the absence of metal does not change the surface morphology. After metal assisted etching a system of nanopores and nanowires was formed. The exact structure of the observed nanowires and the channels between them, as shown e.g. in Figs. 3(b) and (c), depended on the distribution of metal before etching, the etching conditions as well as the drying regimen employed after etching and rinsing. Nonetheless, the images in Fig. 3 are representative of the types of structures observed before and after etching with each type of metal. Here we do not investigate this structure in detail. However, the features shown in Fig. 3(c) that are etched in the rough chunks are quite similar to structures observed when etching wafers with flat surfaces. This indicates that the crystalline structure of the chunk, the nature of the metal/silicon interface, and the etch chemistry are more important for determining the ultimate structure of the etched film than is the initial structure of the Si surface. Figure 3 demonstrates for the first time that V_2O_5 + HF(aq) can be used to form Si nanowires just as has been reported for HOOH + HF(aq). The channels revealed in Fig. 3(c) are directed along the $\langle 110 \rangle$ direction. In metal assisted etching of planar Si wafers using HOOH + HF(aq), the preferred direction of etching is the $\langle 100 \rangle$ though this can be changed to the $\langle 111 \rangle$ family of directions by changing the etchant composition [15].

Kinetics of VO_2^+ to VO^{2+} Conversion by UV/Vis Spectroscopy

The kinetics of hole injection by VO_2^+ into the Si valence band can be followed by absorption spectroscopy. We have previously reported that during stain etching with V_2O_5 + HF solutions, hole injection follows pseudo-first order kinetics when a large surface area sample of silicon chunks is etched

[39,51]. For all of the metal-coated samples investigated here, we also observed pseudo-first order kinetics during metal assisted etching. Figure 4 displays a typical fit of the data to first-order kinetics for both the decay of the V(V) species and the growth of the reduced V(IV) species.

By measuring the mass of Si before and after etching, we also determined the etch stoichiometry. The results for both etch rate and stoichiometric ratios depended on the identity of the metal. These results are summarized in Table 1. The stoichiometries represent means of between 3 and 9 independent experiments and their uncertainties are reported at 95% confidence intervals. The uncertainties in the rate constants are derived from fits that inherently have the potential for greater systematic error. The uncertainties are reported as standard deviations. The pseudo-first order rate constants reported in Table 1 were normalized to the initial mass of Si under the assumption that the mass was proportional to the initial surface area. This did not affect the order of the kinetics but it did make comparisons between different runs more consistent.

Kinetics of H_2 Evolution in V_2O_5 + HF etchants

Hydrogen gas evolution was shown to follow pseudo-first-order kinetics for stain etching in a V_2O_5 + HF [39]. The relative stoichiometry of H_2 formation compared to Si etching was determined by a combination of pressure rise and gravimetric measurements. The evolution of H_2 gas in metal assisted etching exhibited a striking dependence on the identity of the metal. As shown in Figure 5, H_2 evolution from Ag-coated silicon was well described by pseudo-first-order kinetics. For a Au-coated surface pseudo-first-order kinetics with the same rate constant was also observed. However, this rate was attained after an induction period in which the rate was initially somewhat slower. This induction period (15–30 min) was relatively short compared to the usual length of an experiment (120–240 min). Pt-coated surfaces evolved so little H_2 that it was more difficult to evaluate, as shown in Fig. 5(b). H_2 production was roughly constant over time but the amount produced was very low compared to the extent of etching. Pd-coated surfaces again acted much differently, as shown in Fig. 5(c). Initially, in the first two hours of etching they produced virtually no hydrogen. Subsequently, a significant amount of H_2

was evolved at a rate only somewhat lower than that of the Ag- and Au-coated surfaces. To confirm the time-dependent nature of this system, two experimental runs were terminated in the period of little-to-no H_2 production and seven were run to the full duration displayed in Fig. 5(c). If etching was terminated in the early stages, the absence of PL indicated that no microporous Si was formed. After 3 to 4 hours of etching, weak visible PL was observed. For all other metals, visible PL was observed any time enough etching had been performed to produce a color change in the surface of the material. It must be emphasized that because of the variable nature of H_2 production, bubble formation is a very poor proxy for the rate of etching.

Kinetics of H_2 Evolution in HOOH + HF etchants

Unfortunately, the kinetics of hole injection in HOOH + HF cannot be followed in real time by absorption spectroscopy. We attempted two other methods of quantifying the amount of HOOH before and after etching. While this would not allow us to determine the etch kinetics directly as shown in Fig. 4 for V_2O_5, it would allow us to determine the stoichiometry. The two methods used were (1) to titrate against $KMnO_4$ [66] and (2) to measure O_2 evolution caused by catalytic HOOH decomposition in the presence of MnO_2 [67]. Both of these methods allowed us to quantitatively determine HOOH concentrations in our reagents. However, we were unable to obtain consistent results even after many repeated attempts for metal assisted etching. Etching with V_2O_5 never exhibited such irreproducibility. Therefore we conclude that the variability of the n(HOOH)/n(Si) ratio is inherent to the HOOH-based MAE system.

We also attempted to determine the H_2 to Si stoichiometric ratio by the same method as employed above for V_2O_5. Yet again, we were unable to obtain consistent, reproducible results. Therefore, we conclude that the irreproducibility must be inherent to the HOOH + HF metal assisted etching system. The rate of etching in this system must be so dependent on temperature, composition, partial pressures, metal dispersion, pH, surface coverage, surface contamination, side reactions, etc. that we found it impossible to obtain kinetic data of similar quality and reliability as that acquired for the V_2O_5 system.

In addition, it should be noted that a number of metal-nanoparticle-catalyzed side reactions are possible in any system containing HOOH, O_2 and H_2. These side reactions lead to irreconcilable complications with our methods of quantitation.

Discussion

The rate constant for VO_2^+ consumption (which is equal to the rate of VO^{2+} formation) was measured directly by time-dependent absorbance measurements for all systems except Ag. For Ag, absorbance before and after etching was measured. In addition for Ag, the overall rate of consumption can be calculated from the H_2 evolution rate and the reaction stoichiometries since both were constant as etching proceeded. Table 1 summarizes our kinetics results. The rate of VO_2^+ consumption is equal to the rate of hole injection into the Si valence band. The rate of hole injection controls the rate of metal assisted etching. The metals all catalyzed the injection of holes into the Si. Importantly, the rate of hole injection follows smooth first-order kinetics with a fixed rate constant in all cases. For MAE in the presence of Ag, Au, Pd and Pt the hole injection rate was 5 times faster than for stain etching. However, since only ~5% of the plan view surface area of the substrate was covered by metal, the rate of MAE per unit area of metal was roughly 100 times faster than the rate of stain etching. We believe that the constant rate found for all four metals indicated that the measured hole injection rate was diffusion limited in all four cases.

Metal Assisted Etching with Ag and Au

The behavior of Ag- and Au-coated surfaces was very similar. Both exhibited the same stoichiometries as stain etching in the absence of metal. Both also produce microporous Si that exhibited visible PL much like conventionally stain-etched Si. Therefore, the steps of the etching reactions in the presence of Ag and Au nanoparticles are chemically analogous to when the nanoparticles are absent. As we have shown previously [39], this mechanism shares much in common with anodic etching in the current doubling regime (valence 2). However, the counter reaction involves the consumption of an

electron by the oxidant, as described in reactions (1) and (2). Therefore the overall reaction is a valence two reaction

$$Si + 2HF + 2HF_2^- + 2VO_2^+ + 2H^+ \rightarrow SiF_6^{2-} + 2VO^{2+} + H_2(g) + 2H_2O. \qquad (5)$$

The molar stoichiometry with respect to V(V) consumption is $VO_2^+/Si = 2$ and with respect to hydrogen evolution is $H_2/Si = 1$.

The increased rate of reaction in the presence of Ag and Au catalysts was reflected in increased Si consumption, increased H_2 production and an enhancement of the hole injection rate. Since hole injection is the rate limiting step [40], it is the increased rate of hole injection that increases Si consumption (etching) and H_2 production. The increased hole injection rate is caused by the higher density of states near the Fermi energy in the metals as compared to Si, which has essentially no density of states there.

Metal Assisted Etching with Pt

Metal assisted etching in the presence of Pt exhibited statistically the same rate of hole injection as Ag and Au but a different stoichiometry with respect to V(V) consumption $VO_2^+/Si = 3.9 \pm 0.3$. H_2 evolution was just above the measurable limit even though the hole injection exhibited a substantial first-order rate constant. This stoichiometry is indicative of a mixture of nearly all valence 4 etching reactions occurring concurrently with a small amount of valence 2 reaction. There are two different valence 4 reaction pathways. One is the stain-etching analog of the current-quadrupling path found in anodic etching. The second path is electrochemical oxide formation followed by chemical removal of the oxide by HF(aq), which we denote electropolishing. While these two reactions are different mechanistically, overall both reactions have the same stoichiometry,

$$Si + 4VO_2^+ + 2HF + 2HF_2^- + 4H^+ \rightarrow SiF_6^{2-} + 4VO^{2+} + 4H_2O, \qquad (6)$$

with molar stoichiometry $n(VO_2^+)/n(Si) = 4$ and $n(H_2)/n(Si) = 0$. Therefore, stoichiometry alone cannot be used to distinguish between these two reaction mechanisms.

Metal assisted etching in the presence of Pt was dominated by the valence 4 reaction paths. The observation of visible photoluminescence confirmed the formation of nanoporous Si with Pt MAE. Therefore, the current-quadrupling path, which forms nanoporous Si, must occur and electropolishing cannot occur exclusively. Note that because the overall rate of etching as defined by the rate of Si atom removal was the same for Ag, Au and Pt, the shift of mechanism was inherent to the chemical identity of the metal. The change in stoichiometry was not caused by a kinetic effect analogous to "etching beyond the critical current density" since the rate of hole injection and coverage of metal is roughly the same in all cases.

Metal Assisted Etching with Pd

The stoichiometry and reaction mechanism of in the presence of Pd was more complex than for the other three metals. Initially the reaction was dominated by a valence 4 path with $n(VO_2^+)/n(Si) \approx 4$ and $n(H_2)/n(Si) \approx 0$. However at long times the stoichiometry became mixed with $n(VO_2^+)/n(Si) \approx 3$ and $n(H_2)/n(Si) \approx 0.5$, which can be explained by concurrent etching along both the valence 4 and valence 2 paths. At early times no nanoporous Si was formed in the presence of Pd. Therefore, electropolishing was the dominant valence 4 process at early times and no nanoporous Si exhibiting visible PL was formed. At long times, the surface became rough. The Pd nanoparticles continued to catalyze electropolishing in their vicinity. However, ridges removed from the Pd nanoparticles were subjected to slower conventional stain etching. This causes a mixed valence overall etch stoichiometry to be observed at long times.

Metal Dependent Etch Mechanism

How does the chemical identity of the metal change the stoichiometry and, therefore, the mechanism of the reactions involved in metal assisted etching? The hole injection step is what controls the rate and this step is, in turn, controlled by the electronic structure of the metal and the metal/Si interface. Kolasinski [68] has recently calculated the band bending inherent to the metal/Si interface for Ag, Au, Pt and Pd. It is commonly proposed in the literature that holes injected by the oxidant into the metal diffuse

from the metal into the Si. Etching then occurs according to the three pathways (current doubling, current quadrupling and electropolishing) delineated above once the hole has been injected into Si.

First, the conventional explanation is contradicted by the fact that hole injection occurs primarily at the Fermi level of the metal and that the Fermi energy of the metal lies above the valence band maximum of Si. Since holes relax to the top of a band, there is no driving force for them to leave the metal. Furthermore, the band bending is such that for none of the four metals is the hole more stable in the Si than either in the metal or at the metal/Si interface. Second, the conventional mechanism does not explain why an etch track forms *below* the metal nanoparticle (a region not exposed to the solution) but por-Si forms away from the nanoparticle. Third, it does not explain why electropolishing, which is required to form an etch track, occurs next to the nanoparticle while por-Si formation occurs remotely from the nanoparticle.

The formation of both etch track pores and porous Si away from the metal particles requires that etching be made "nonlocal," that is, that it must occur not only at the location of the metal nanoparticle but also remotely. The work of Chiappini et al. [69] and Geyer et al. [70,71] addressed the need for nonlocal etching by considering the dissolution and redeposition of the metal. Dissolution and redeposition is well documented for Ag; however, it is not evident for Au, Pd and Pt [9] when HOOH is used as the oxidant. Furthermore, because of the lower electrochemical potential of VO_2^+, application of the Nernst equation shows that Au cannot be dissolved and Pt can only be minimally dissolved when VO_2^+ is used as the oxidant. Since both Ag and Au exhibit the same stoichiometry, it appears either (1) that dissolution and redeposition do not play a role, or (2) that dissolution and redeposition do not alter the mechanism of the etching processes and are not essential for local and nonlocal etching.

Kolasinski [68] has proposed that it is the polarization induced by an excess of holes on the metal and/or at the metal/Si interface that causes etching. A charge imbalance caused by hole injection into the metal nanoparticle turns the nanoparticle into a localized power supply. This model requires a detailed

calculation of the charge distribution at the metal/Si interface and its screening by the metal nanoparticle, the Si bulk and the solution. Nonetheless, the introduction of metal-dependent interface electronic structure and the concomitant electric field distribution in its vicinity have several appealing features to explain metal assisted etching in general and metal-dependent etch mechanisms.

A charged metal nanoparticle produces an electric field that drops in strength as distance from the nanoparticle increases. Therefore, the effective electric field near the nanoparticle can be in the electropolishing regime, while further away the polarization corresponds to the por-Si formation regime. Thus, nanoporous Si can be formed remotely from the nanoparticle, which will facilitate etchant transport to the metal/Si interface, which then allows electropolishing to form the etch track of the metal nanoparticle. The balance between por-Si formation and electropolishing depends on the exact nature of the metal/Si electronic structure and the charge imbalance that it supports on the nanoparticle. Therefore, the stoichiometry of the etch reactions should unsurprisingly depend on the chemical identity of the metal. The reactivity of the various metals might also depend on the size and structure of the metal nanoparticles. A systematic study of reaction rates and stoichiometries would be required to determine the detailed influence of nanoparticle size and structure.

Conclusion

The stoichiometry of etching in V_2O_5 + HF depends on the metal used as a catalyst. The presence of Ag and Au nanoparticles causes etching to exhibit molar ratios of roughly 2:1 for $n\left(\mathrm{VO_2^+}\right)/n(\mathrm{Si})$ and approximately 1:1 for $n\left(\mathrm{H_2}\right)/n(\mathrm{Si})$. These stoichiometries are the same as those exhibited by stain etching in the absence of metals. The photoluminescence and structure of these films is different from films produced in the absence of the catalyst; nonetheless, the mechanism of etching is the same. Put differently, the spatial character of etching is different with and without the presence of Ag or Au, but the chemistry itself does not change.

Etching in the presence of Pd and Pt nanoparticles exhibits stoichiometries that differ from Ag and Au as well as from each other. For Pt, $n(VO_2^+)/n(Si) \approx 4$ and $n(H_2)/n(Si) \approx 0$. Pd etches initially with the same stoichiometry as Pt; however, whereas etching with Pt creates brightly photoluminescent nanoporous Si, initial etching with Pd does not. Therefore, Pt catalyzed etching is dominated by current-quadrupling etching whereas Pd catalyzed etching is dominated by electropolishing. The introduction of a good hydrogen recombination catalyst (Pt and Pd) as opposed to a poor hydrogen recombination catalyst (e.g. Ag and Au) changes the mechanism of etching as compared to stain etching. The dependence of the etch mechanism and the balance between valence 2 and valence 4 processes is ascribed to the dependence of the electronic structure of the metal/Si interface (and the resulting polarization of the surrounding Si) on the chemical identity of the metal and the charge imbalance created by hole injection by the oxidant into the metal.

The HOOH + HF system is inherently more nonlinear and not kinetically well behaved. This is caused by much greater sensitivity to reaction conditions (e.g. amount and structure of metal deposited, temperature, composition including the concentrations of reaction products, specific adsorption leading to dependence of reaction rates on surface coverages rather than solution concentrations directly, etc.) and the interference of competing reactions involving H_2, O_2, H_2O and HOOH.

Acknowledgments

We thank James Falcone for providing the reclaim wafer chunks. Nathan Noyes and Abbie Ganas assisted with the preparation of some samples. Supported by West Chester University, Pennsylvania State System of Higher Education, and the Center for Microanalysis and Imaging, Research and Training (CMIRT) at WCU and the Institute of Materials Science at UConn.

References

[1] K.W. Kolasinski, Curr. Opin. Solid State Mater. Sci. 9 (2005) 73.

[2] K.W. Kolasinski, in: L.T. Canham (Ed.), Handbook of Porous Silicon, Springer Verlag, Berlin, 2014, p. 35.

[3] K.W. Kolasinski, in: P. Granitzer, K. Rumpf (Eds.), Nanostructured Semiconductors: From Basic Research to Applications, Pan Stanford Publishing, Singapore, 2014, p. 45.

[4] C.S. Fuller, J.A. Ditzenberger, J. Appl. Phys. 27 (1957) 544.

[5] D.R. Turner, J. Electrochem. Soc. 107 (1960) 810.

[6] R.J. Archer, J. Phys. Chem. Solids 14 (1960) 104.

[7] C.M.A. Ashruf, P.J. French, P.M.M.C. Bressers, J.J. Kelly, Sens. Actuators A 74 (1999) 118.

[8] J.J. Kelly, X.H. Xia, C.M.A. Ashruf, P.J. French, IEEE Sensors J. 1 (2001) 127.

[9] X. Li, P.W. Bohn, Appl. Phys. Lett. 77 (2000) 2572.

[10] S. Chattopadhyay, P.W. Bohn, J. Appl. Phys. 96 (2004) 6888.

[11] K. Tsujino, M. Matsumura, Adv. Mater. 17 (2005) 1045.

[12] Z.P. Huang, T. Shimizu, S. Senz, Z. Zhang, X.X. Zhang, W. Lee, N. Geyer, U. Gösele, Nano Lett. 9 (2009) 2519.

[13] Z.P. Huang, X.X. Zhang, M. Reiche, L.F. Liu, W. Lee, T. Shimizu, S. Senz, U. Gösele, Nano Lett. 8 (2008) 3046.

[14] S.P. Scheeler, S. Ullrich, S. Kudera, C. Pacholski, Nanoscale Res. Lett. 7 (2012) 450.

[15] Z. Huang, N. Geyer, P. Werner, J. de Boor, U. Gösele, Adv. Mater. 23 (2011) 285.

[16] X.L. Li, Curr. Opin. Solid State Mater. Sci. 16 (2012) 71.

[17] M.-L. Zhang, K.-Q. Peng, X. Fan, J.-S. Jie, R.-Q. Zhang, S.-T. Lee, N.-B. Wong, J. Phys. Chem. C 112 (2008) 4444.

[18] K.-Q. Peng, Y.-J. Yan, S.-p. Gao, J. Zhu, Adv. Mater. 14 (2002) 1164.

[19] K.Q. Peng, A.J. Lu, R.Q. Zhang, S.T. Lee, Adv. Func. Mater. 18 (2008) 3026.

[20] S.W. Schmitt, F. Schechtel, D. Amkreutz, M. Bashouti, S.K. Srivastava, B. Hoffmann, C. Dieker, E. Spiecker, B. Rech, S.H. Christiansen, Nano Lett. 12 (2012) 4050.

[21] J.D. Holmes, K.P. Johnston, R.C. Doty, B.A. Korgel, Science 287 (2000) 1471.

[22] I. Ponomareva, M. Menon, D. Srivastava, A.N. Andriotis, Phys. Rev. Lett. 95 (2005) 265502.

[23] A.I. Hochbaum, R.K. Chen, R.D. Delgado, W.J. Liang, E.C. Garnett, M. Najarian, A. Majumdar, P.D. Yang, Nature (London) 451 (2008) 163.

[24] F. Peng, Y.Y. Su, Y.L. Zhong, C.H. Fan, S.T. Lee, Y. He, Acc. Chem. Res. 47 (2014) 612.

[25] Y. He, Y.L. Zhong, F. Peng, X.P. Wei, Y.Y. Su, S. Su, W. Gu, L.S. Liao, S.T. Lee, Angew. Chem., Int. Ed. Engl. 50 (2011) 3080.

[26] K.Q. Peng, X. Wang, X.L. Wu, S.T. Lee, Nano Lett. 9 (2009) 3704.

[27] S.W. Boettcher, J.M. Spurgeon, M.C. Putnam, E.L. Warren, D.B. Turner-Evans, M.D. Kelzenberg, J.R. Maiolo, H.A. Atwater, N.S. Lewis, Science 327 (2010) 185.

[28] S. Hu, M.R. Shaner, J.A. Beardslee, M. Lichterman, B.S. Brunschwig, N.S. Lewis, Science 344 (2014) 1005.

[29] X. Wang, K.Q. Peng, X.J. Pan, X. Chen, Y. Yang, L. Li, X.M. Meng, W.J. Zhang, S.T. Lee, Angew. Chem., Int. Ed. Engl. 50 (2011) 9861.

[30] K.W. Kolasinski, in: H. Santos (Ed.), Porous silicon for biomedical applications, Woodhead Publishing, London, 2014, p. 52.

[31] Y. Xiu, L. Zhu, D.W. Hess, C.P. Wong, Nano Lett. 7 (2007) 3388.

[32] K. Rykaczewski, O.J. Hildreth, C.P. Wong, A.G. Fedorov, J.H.J. Scott, Nano Lett. 11 (2011) 2369.

[33] V. Schmidt, J.V. Wittemann, U. Gösele, Chem. Rev. 110 (2010) 361.

3 [34] A.I. Hochbaum, D. Gargas, Y.J. Hwang, P. Yang, Nano Lett. 9 (2009) 3550.
4 [35] Y. Cui, Z.H. Zhong, D.L. Wang, W.U. Wang, C.M. Lieber, Nano Lett. 3 (2003) 149.
5 [36] V. Schmidt, J.V. Wittemann, S. Senz, U. Gösele, Adv. Mater. 21 (2009) 2681.
6 [37] K.Q. Peng, Z.P. Huang, J. Zhu, Adv. Mater. 16 (2004) 73.
7 [38] C.R. Becker, S. Apperson, C.J. Morris, S. Gangopadhyay, L.J. Currano, W.A. Churaman, C.R.
8 Stoldt, Nano Lett. 11 (2011) 803.
9 [39] K.W. Kolasinski, W.B. Barclay, Angew. Chem., Int. Ed. Engl. 52 (2013) 6731.
10 [40] K.W. Kolasinski, J.W. Gogola, W.B. Barclay, J. Phys. Chem. C 116 (2012) 21472.
11 [41] K.W. Kolasinski, J.D. Hartline, B.T. Kelly, J. Yadlovskiy, Mol. Phys. 108 (2010) 1033.
12 [42] K.W. Kolasinski, J. Phys. Chem. C 114 (2010) 22098.
13 [43] K.W. Kolasinski, Surf. Sci. 603 (2009) 1904.
14 [44] K.W. Kolasinski, Phys. Chem. Chem. Phys. 5 (2003) 1270.
15 [45] L. Koker, K.W. Kolasinski, J. Phys. Chem. B 105 (2001) 3864.
16 [46] C. Gondek, M. Lippold, I. Röver, K. Bohmhammel, E. Kroke, J. Phys. Chem. C 118 (2014)
17 2044.
18 [47] D.-H. Eom, K.-S. Kim, J.-G. Park, Jpn. J. Appl. Phys. 41 (2002) 5881.
19 [48] E. Skúlason, V. Tripkovic, M.E. Björketun, S. Gudmundsdóttir, G. Karlberg, J. Rossmeisl, T.
20 Bligaard, H. Jónsson, J.K. Nørskov, J. Phys. Chem. C 114 (2010) 18182.
21 [49] E. Santos, P. Quaino, W. Schmickler, Phys. Chem. Chem. Phys. 14 (2012) 11224.
22 [50] C. Carraro, R. Maboudian, L. Magagnin, Surf. Sci. Rep. 62 (2007) 499.
23 [51] K.W. Kolasinski, W.B. Barclay, ECS Trans. 50 (2013) 25.
24 [52] L. Magagnin, R. Maboudian, C. Carraro, J. Phys. Chem. B 106 (2002) 401.
25 [53] Y.H. Ogata, K. Kobayashi, Curr. Opin. Solid State Mater. Sci. 10 (2006) 163.
26 [54] C. Chartier, S. Bastide, C. Levy-Clement, Electrochim. Acta 53 (2008) 5509.
27 [55] M. Chemla, T. Homma, V. Bertagna, R. Erre, N. Kubo, T. Osaka, J. Electroanal. Chem. 559
28 (2003) 111.
29 [56] P. Gorostiza, P. Allongue, R. Díaz, J.R. Morante, F. Sanz, J. Phys. Chem. B 107 (2003) 6454.
30 [57] K.Q. Peng, J. Zhu, Electrochim. Acta 49 (2004) 2563.
31 [58] Z.P. Huang, T. Shimizu, S. Senz, Z. Zhang, N. Geyer, U. Gösele, J. Phys. Chem. C 114 (2010)
32 10683.
33 [59] R.G. Milazzo, G. D'Arrigo, C. Spinella, M.G. Grimaldi, E. Rimini, J. Electrochem. Soc. 159
34 (2012) D521.
35 [60] F. Shi, Y.Y. Song, H. Niu, X.H. Xia, Z.Q. Wang, X. Zhang, Chem. Mater. 18 (2006) 1365.
36 [61] Y.Y. Song, Z.D. Gao, J.J. Kelly, X.H. Xia, Electrochem. Solid State Lett. 8 (2005) C148.
37 [62] Y. Wang, M. Becker, L. Wang, J.Q. Liu, R. Scholz, J. Peng, U. Gösele, S. Christiansen, D.H.
38 Kim, M. Steinhart, Nano Lett. 9 (2009) 2384.
39 [63] S. Yae, M. Tashiro, M. Abe, N. Fukumuro, H. Matsuda, J. Electrochem. Soc. 157 (2010) D90.
40 [64] M.E. Dudley, K.W. Kolasinski, Electrochem. Solid State Lett. 12 (2009) D22.
41 [65] M.E. Dudley, K.W. Kolasinski, Phys. Status Solidi A 206 (2009) 1240.
42 [66] D.A. Skoog, D.M. West, F.J. Holler, Fundamentals of Analytical Chemistry, Saunders College
43 Publishing, Fort Worth, TX, 1996.
44 [67] F.A. Cotton, G. Wilkinson, Advanced Inorganic Chemistry, John Wiley & Sons, New York,
45 1972.
46 [68] K.W. Kolasinski, Nanoscale Res. Lett. 9 (2014) 432.
47 [69] C. Chiappini, X.W. Liu, J.R. Fakhoury, M. Ferrari, Adv. Func. Mater. 20 (2010) 2231.
48 [70] N. Geyer, B. Fuhrmann, H.S. Leipner, P. Werner, ACS Appl. Mater. Interfaces 5 (2013) 4302.
49 [71] N. Geyer, B. Fuhrmann, Z.P. Huang, J. de Boor, H.S. Leipner, P. Werner, J. Phys. Chem. C 116
50 (2012) 13446.
51
52
53
54
55
56
57
58
59
60
61
62
63
64
65

Figure Captions

Figure 1. Secondary electron SEM micrographs and particle size distributions for (a, b) Ag, (c, d) Pd, (e, f) Pt and (g, h) Au deposited galvanically on Si chunks. The distributions represent a minimum of 250 measurements of particle/cluster diameters in each case.

Figure 2. Photoluminescence spectra acquired with excitation at 350 nm. Both samples had Pt nanoparticles deposited prior to etching. The PL from the HOOH + HF etched sample is clearly red shifted and much broader as well as less intense than the PL from the sample etched in V_2O_5 + HF.

Figure 3. SEM micrograph of Si chunk before (a) and after (b) Ag MAE. (c) A TEM micrograph of a FIB lifted section after Ag MAE revealing parallel nanopores below the irregular surface of the Si chunk. V_2O_5 dissolved in HF(aq) was used as the etchant.

Figure 4. Absorbance data indicates that both the disappearance of VO_2^+ and the appearance of VO^{2+} follow first order kinetics. This example is for etching in a V_2O_5 + HF solution. The Si surface has had Pt nanoparticles deposited on it prior to etching. Similar pseudo-first-order behavior is found for Ag, Au and Pd metal assisted etching in V_2O_5 + HF.

Figure 5. H_2 evolution during the metal assisted etching of Si in V_2O_5 + HF solution. H_2 is produced according to pseudo-first-order kinetics. (a) Ag/Si. (b) Pt/Si. (c) Pd/Si. In each case the pressure is measured from before the stopper is placed on the reaction vessel (indicated by sudden jump in pressure) until the stopper is removed (indicated by the sudden drop).

Table

Table 1. Stoichiometric coefficients and pseudo-first order rate constants for etching in V_2O_5 + HF solutions. V/Si = moles VO_2^+ consumed / moles Si etched. H_2/Si = moles H_2 evolved / moles Si etched. k_V is the rate constant for VO_2^+ consumption. k_{H2} is the rate constant for H_2 evolution. Stain refers to etching in the absence of metal nanoparticles.

	V/Si	H_2/Si	k_V(25°C) / s^{-1} g^{-1}	k_{H2}(25°C) / s^{-1} g^{-1}
Stain	1.98±0.13	1.01±0.08	$(4.0\pm1.2) \times 10^{-5}$	$(1.9\pm0.8) \times 10^{-5}$
Ag	2.1±0.4	0.89±0.03	$(2.1\pm0.8) \times 10^{-4}$	$(9\pm3) \times 10^{-5}$
Au	2.0±0.2	0.94±0.02	$(1.8\pm0.4) \times 10^{-4}$	$(9\pm2) \times 10^{-5}$
Pd	3.0±0.5*	0.51±0.09*	$(2.1\pm0.1) \times 10^{-4}$	$(7.2\pm1.2) \times 10^{-5}$*
Pt	3.9±0.3	0.2±0.2	$(2.1\pm0.1) \times 10^{-4}$	$(4\pm4) \times 10^{-5}$

*These values are evaluated at long times.

Figure 1

Click here to download high resolution image

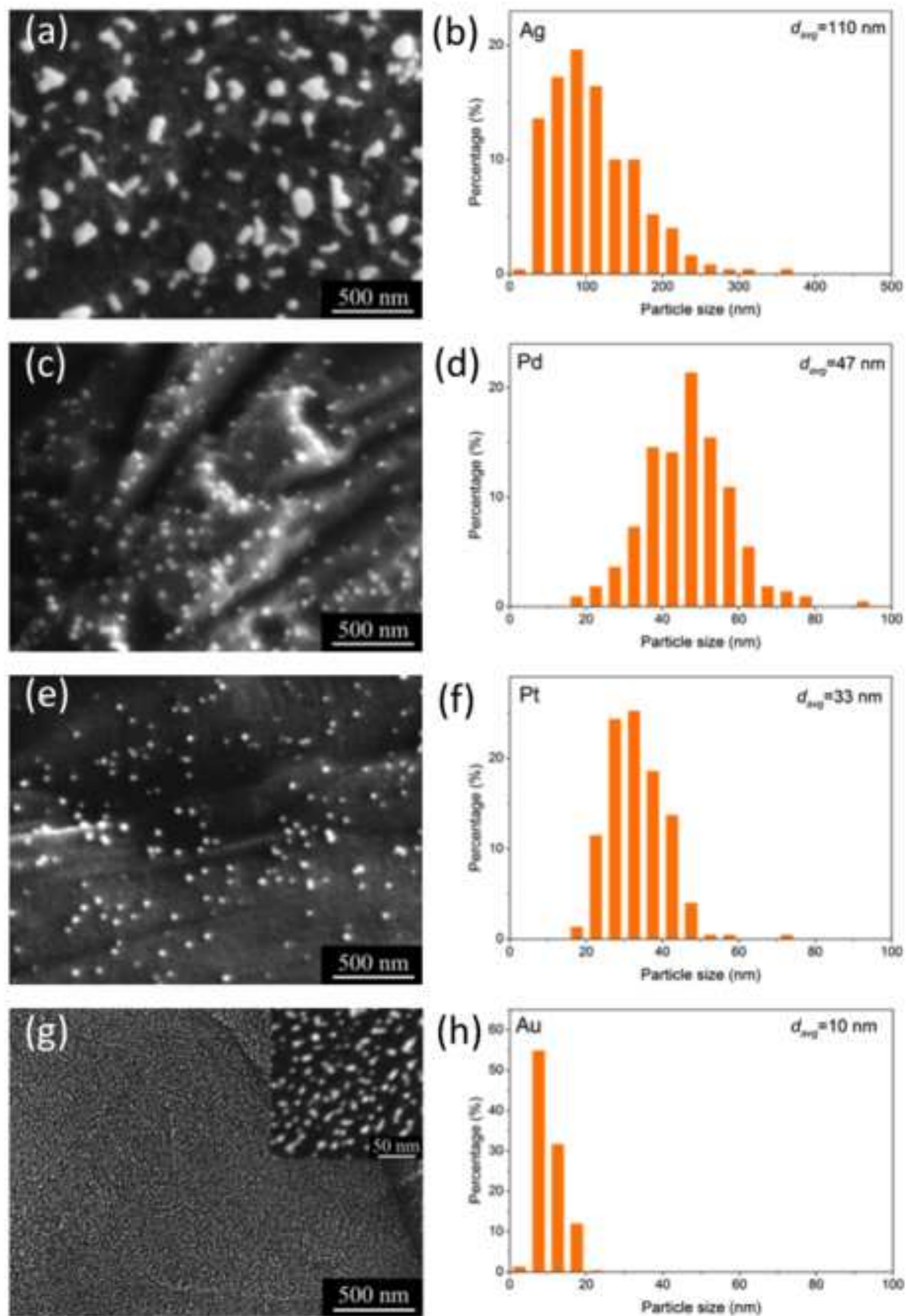

Figure 2
Click here to download high resolution image

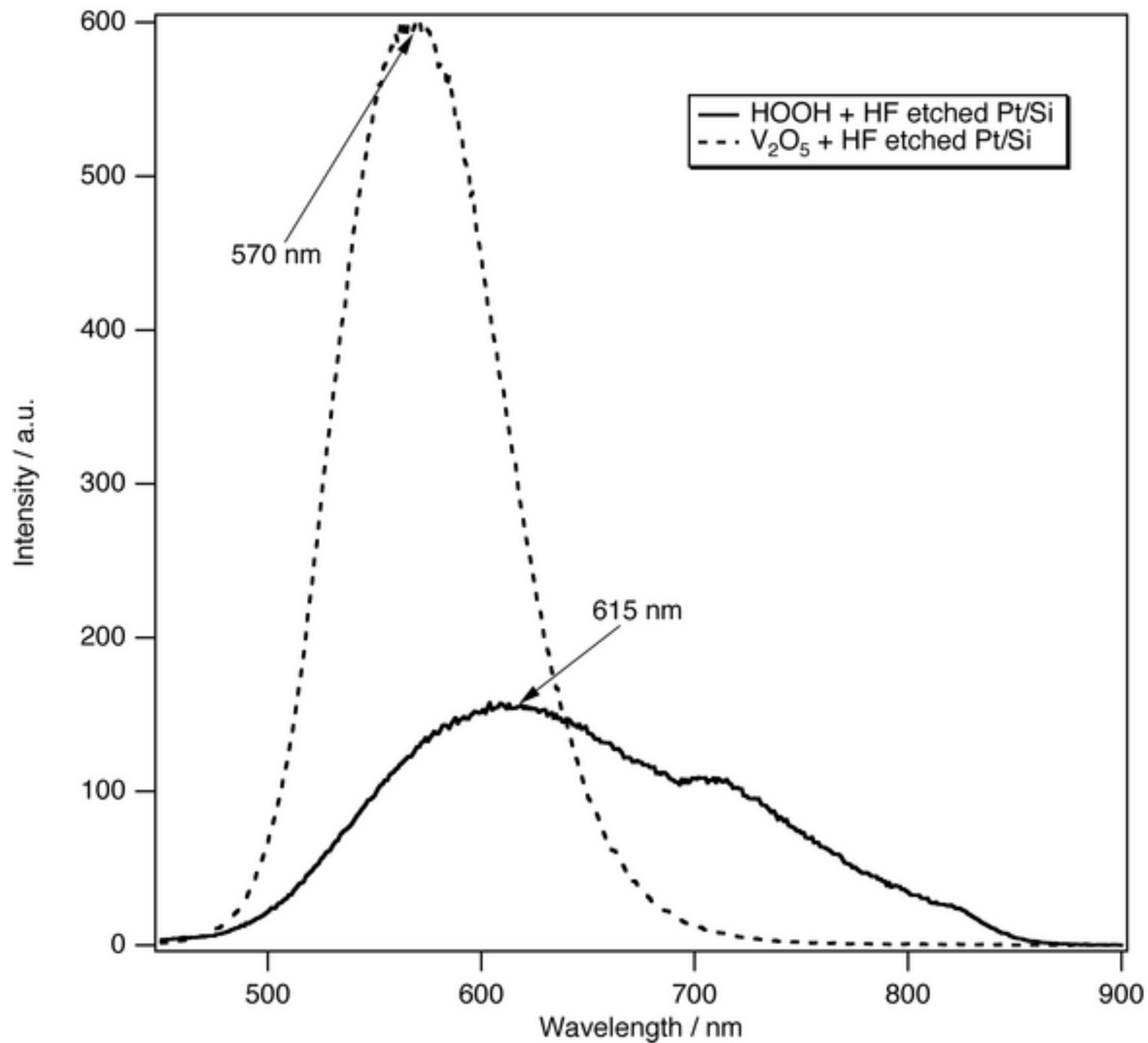

Figure 3

Click here to download high resolution image

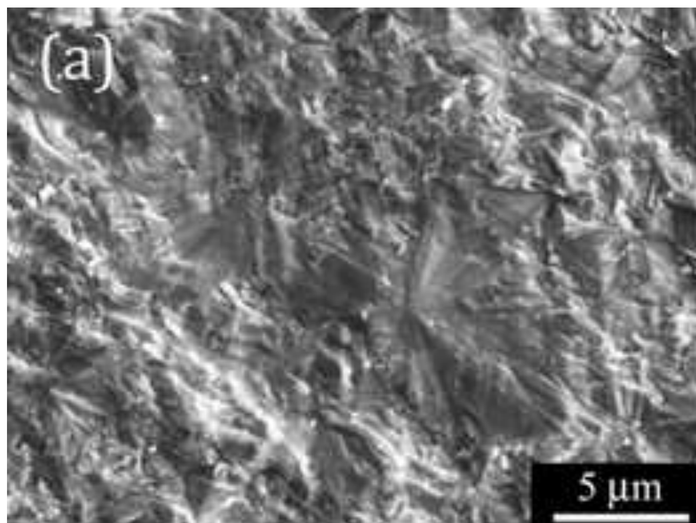

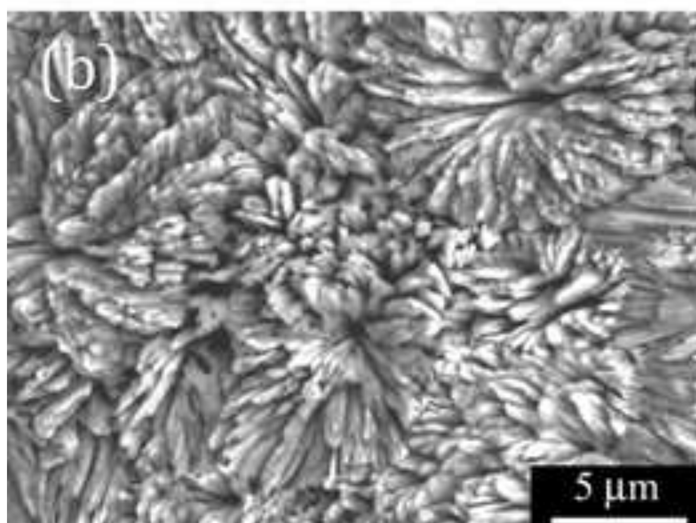

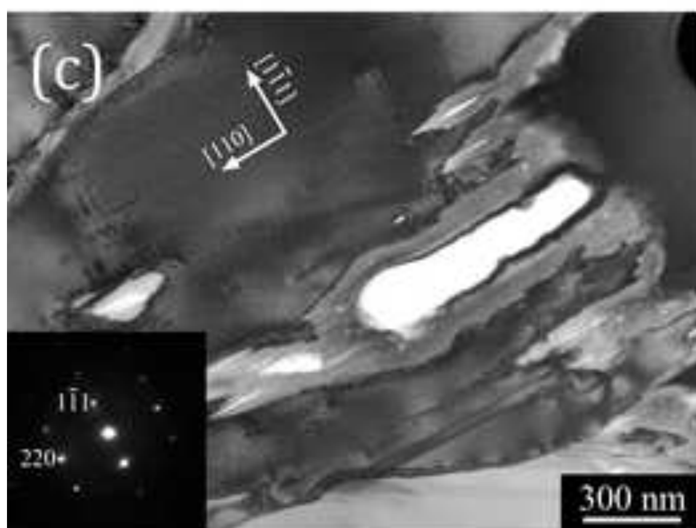

Figure 4
Click here to download high resolution image

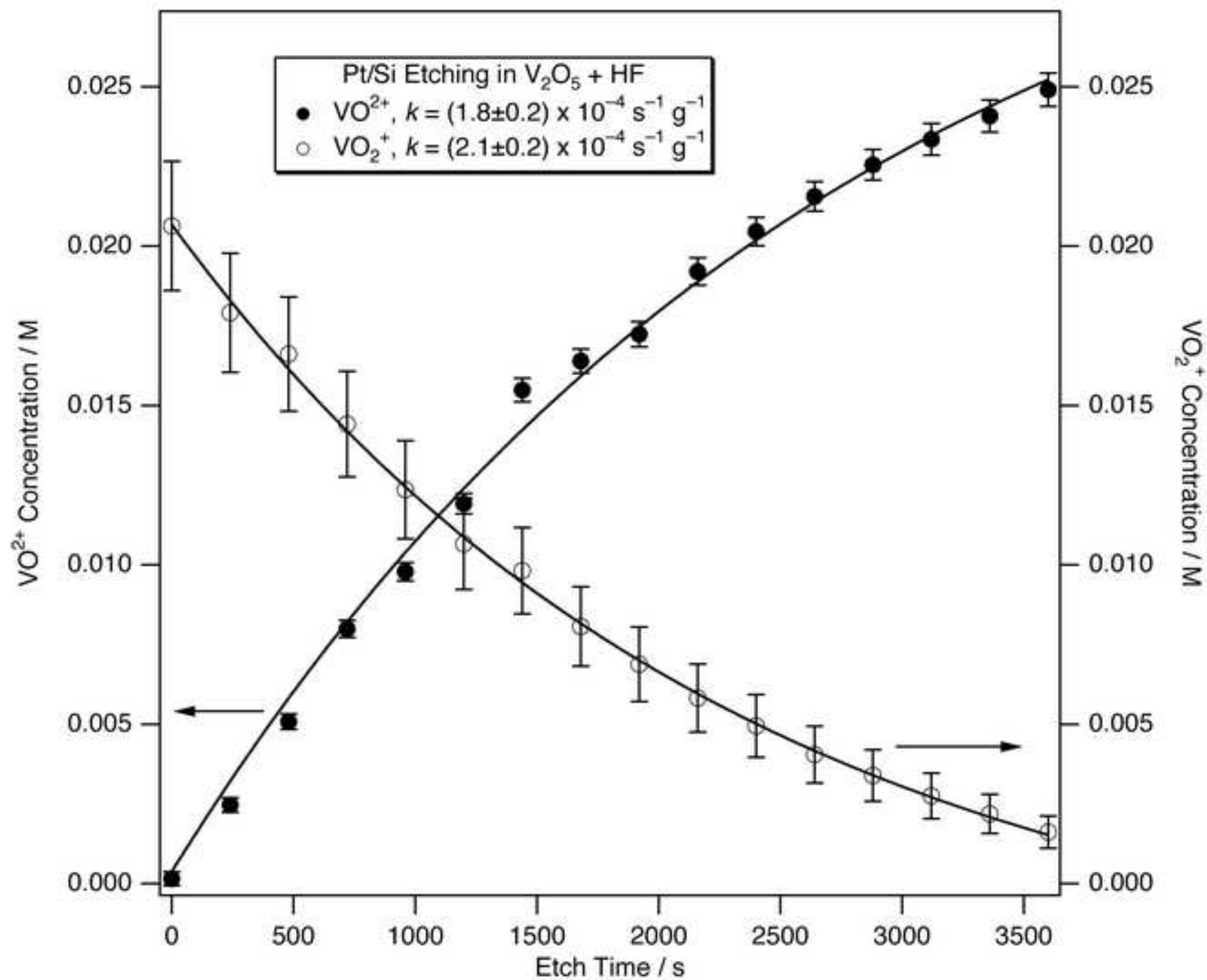

Figure 5a

Click here to download high resolution image

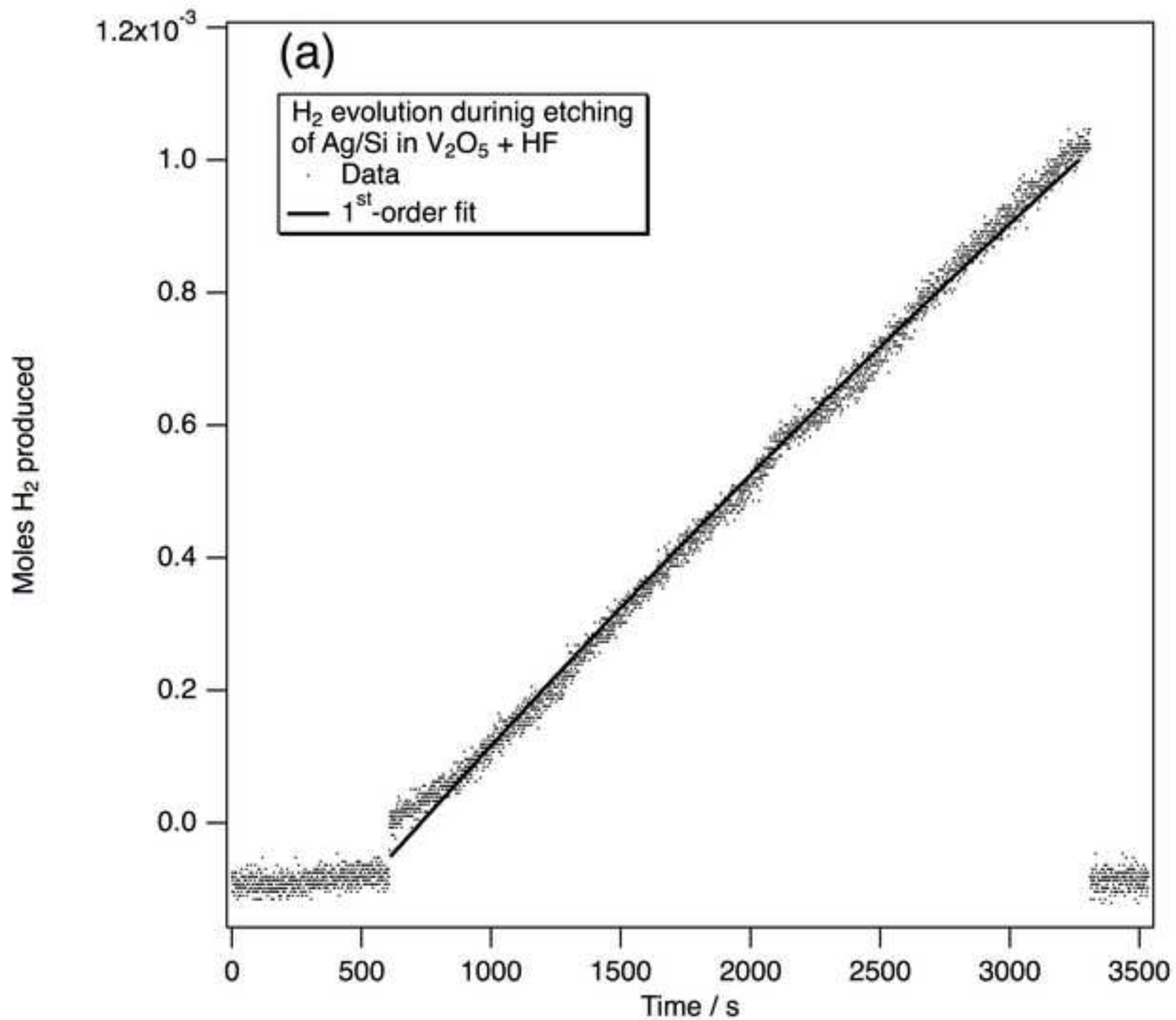

Figure 5b

Click here to download high resolution image

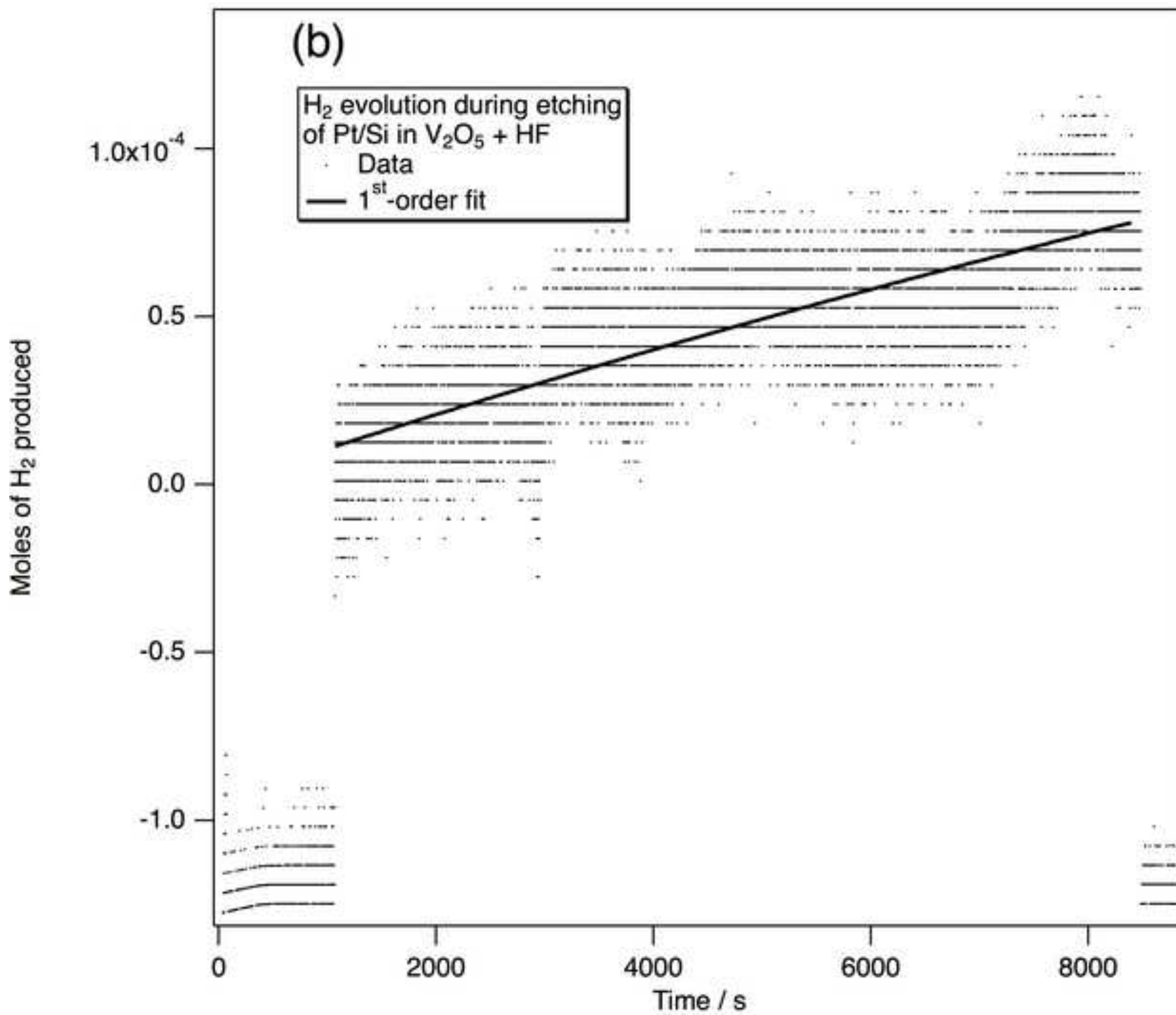

Figure 5c

Click here to download high resolution image

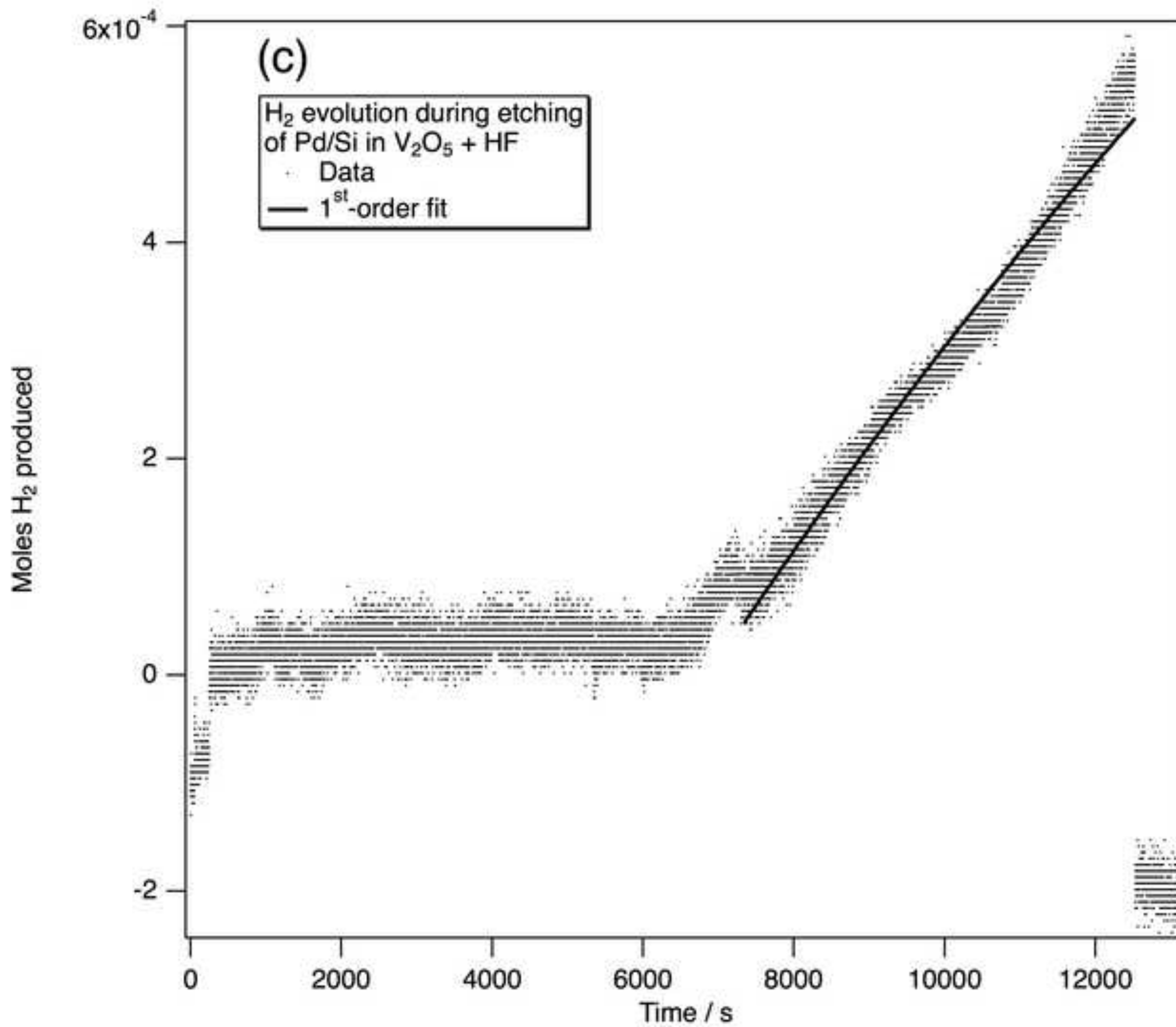

Revisions Highlighted

Click here to download Supplementary Materials: PA-14-04419 Revisions Highlighted.pdf